Structural Analysis of Mono-Substituted N-butyl-pyridinium Salts: In Search of Ionic Liquids

Steven P. Kelley – University of Missouri
Volodymyr Smetana – Stockholm University
Anja-Verena Mudring – Stockholm University
Robin D. Rogers – University of Alabama

Citation of published version:
Kelley, S., Smetana, V., Mudring, A., Rogers, R. (2021): Structural Analysis of Mono-Substituted N-butyl-pyridinium Salts: In Search of Ionic Liquids. *Journal of Coordination Chemistry*. 74(1-3).

DOI: https://doi.org/10.1080/00958972.2021.1876851

JOURNAL OF COORDINATION CHEMISTRY
2021, VOL. 74, NOS. 1–3, 117–128
https://doi.org/10.1080/00958972.2021.1876851

Structural analysis of mono-substituted *N*-butyl-pyridinium salts: in search of ionic liquids

Steven P. Kelley[a], Volodymyr Smetana[b], Anja-Verena Mudring[b] and Robin D. Rogers[b,c]

[a]Department of Chemistry, University of Missouri, Columbia, MO, USA; [b]Department of Materials and Environmental Chemistry, Stockholm University, Stockholm, Sweden; [c]College of Arts and Sciences, The University of Alabama, Tuscaloosa, AL, USA

ABSTRACT

Four mono-substituted *N*-butylpyridinium salts, 1-butyl-4-dimethylaminopyridinium chloride [b4dmapy]Cl, 1-butyl-4-methyl-pyridinium bromide [b4mpy]Br, 1-butyl-4-methylpyridinium hexa-fluorophosphate [b4mpy][PF_6], and 1-butyl-3-methylpyridinium hexafluorophosphate [b3mpy][PF_6] were synthesized and character-ized using single crystal X-ray diffraction. The crystal structures were examined with the intent of identifying ion interactions leading to higher melting points of the halide salts with respect to the $[PF_6]^-$ salts. The changes in hydrogen bonding, C–H···π, and van der Waals interactions have been analyzed with respect to anion, functional groups, and the symmetry of the cation to establish interdepend-ence with the compound's physicochemical properties. It has been observed that the cation–anion interactions are represented by highly directional hydrogen bonds and show strong preference to positions of interaction depending on the anion. The cations of the halide salts show strong tendency towards higher dimensional forma-tions, while those of the $[PF_6]^-$ salts prefer low dimensional assemblies both being based mainly on the weaker van der Waals interactions. These interactions depend on the shape of the cation but may offer certain structure-ordering rigidity accommodating variable anions.

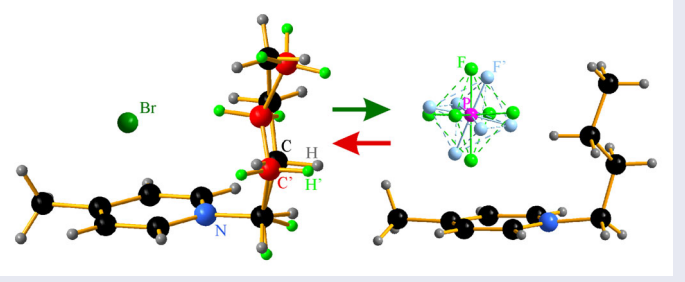

ARTICLE HISTORY
Received 24 November 2020
Accepted 7 January 2021

KEYWORDS
Ionic liquid; crystal structure; symmetry; disorder; bonding

CONTACT Anja-Verena Mudring anja-verena.mudring@mmk.su.se; Robin D. Rogers rdrogers@ua.edu Department of Materials and Environmental Chemistry, Stockholm University, Svante Arrhenius väg 16 C,10691 Stockholm, Sweden

This paper is dedicated to Professor Jerry L. Atwood on the occasion of his retirement. We hope by this time he has forgiven an academic son (RDR) and grandson (SPK) who turned for so long to the dark side of the liquid state of matter.

1. Introduction

Ionic liquids are salts whose melting points are low enough that they can be used in place of molecular liquids; this is frequently considered, though not required, to be a melting point below 100 °C [1]. ILs are now used as replacements for molecular solvents, usually taking advantage of the fact that they have at least two ions that can be tuned independently to control the physicochemical properties. ILs have proven especially useful as solvents and reaction media in coordination chemistry, where they are applied in catalysis [2, 3], separations [4–6], crystal engineering [7, 8], and the synthesis of functional materials [9, 10].

We have been interested in using ILs to discover unprecedented metal–ligand interactions, since most known coordination chemistry is restricted to a relatively small set of molecular solvents, which usually solvate the metal ion through dative bonds and thus directly complete with the target ligand. ILs can solvate metal ions weakly through purely ionic interactions or even allow use of the target ligand as a neat solvent; this has allowed the isolation of a number of metal complexes with normally non-coordinating ligands [11, 12]. The fully ionic nature of ILs as solvents also influences coordination chemistry. This has been particularly well-illustrated in many liquid–liquid extraction studies showing ion exchange reactions [13–16] and speciation dominated by ionic metal complexes [17–19], both of which are unusual for nonaqueous solvents. ILs have also been shown to co-crystallize with unusual metal species, in some cases acting as host lattices [20, 21].

While the diversity of ILs makes it easy to incorporate any desired functional group, such as a metal coordination site, it makes it impossible to predict the properties of the IL itself. Investigations of the structures and properties of ILs are therefore needed in order to fully understand processes occurring in solution in ILs. For example, we have observed that dialkylimidazolium acetate ILs readily dehydrate a wide range of metal salts to produce anhydrous, anionic acetate complexes [22]; these ILs are also known to solvate hydrogen bond donors better than metal ions [23], and thus the behavior can be understood by the IL solvating water but allowing crystallization of the weakly basic metal complexes as salts. However, the design space of ILs is vast. In all likelihood most ILs have yet to be discovered, let alone thoroughly characterized.

In this study, we investigate the crystal structures of a family of substituted *N*-butylpyridinium salts in order to better understand the behavior of this cation family and its possible role in facilitating the crystallization of metal complexes. *N*-Alkylpyridinium ILs are well known; they were among the first ILs to be investigated [24], and the cation is common in commercially available ionic liquids owing to its ease of synthesis and potential function as an antimicrobial agent [25]. In our research we have used 4-methyl-*N*-butylpyridinium ($[b4mpy]^+$) ILs to crystallize coordination polymers with the IL anion, where $[b4mpy]^+$ is present as the counterion [26, 27]. However, structurally-characterized examples from this family of salts are surprisingly underreported. The Cambridge Structural Database (CSD) [28] contains just 9 crystal structures of metal-free *N*-butylpyridinium salts [29–35] and only 3 where the pyridinium ring is further functionalized: [b4mpy][PCl_6] [36], 2-methyl-*N*-butylpyridinium bromide ([b2mpy]Br)

[37], and a chloroform solvate of 4-(dimethylamino)-*N*-butylpyridinium chloride ([b4dmapy]Cl·$CHCl_3$) [38]. Here we present the crystal structures of four crystalline *N*-butylpyridinium salts varying in substitution about the ring and in the identity of the counterion. The crystal packing of these salts were analyzed to understand how the interactions of these cations vary with differing shape, symmetry, and electronic properties in order to better predict where they will be useful in crystallizing new coordination complexes.

2. Experimental

3-Methylpyridine, 4-methylpyridine, 4-(dimethylamino)pyridine, 1-chlorobutane, and 1-bromobutane were purchased from Aldrich Chemicals (Milwaukee, WI, USA) and used without purification. Ozark Mahonic (Tulsa, OK, USA) donated the hexafluorophosphoric acid. All chemicals were used as received. The synthesis of all Cl^-, Br^-, and $[PF_6]^-$ salts were performed in the same manner, according to the following general procedure.

The alkyl-pyridine or alkyl-aminopyridine was dissolved in ethyl acetate. After complete dissolution, 1-halogenoalkane was slowly added. The ratio of pyridine to 1-halogenoalkane was 1:1. The reaction mixture was stirred with heating (70 °C) for 1 week. The product phase separated from the reaction mixture. After the reaction was complete, the layers were separated and the product layer was washed three times with fresh ethyl acetate (equal volume compared to product). The product was then dried under high vacuum. After drying, the product was cooled to room temperature at which point it crystallized. Suitable crystals of the 1-butyl-4-methylpyridinium and 1-butyl-4-dimethylaminopyridinium halides for single crystal X-ray diffraction (SCXRD) were chosen from the product.

Caution! Standard safeguard procedures should be followed during the handling of fluorine-containing materials.

Where indicated, the syntheses of the $[PF_6]^-$ salts were conducted as follows. The halide salt was dissolved in water and 1 eqv. of HPF_6 was added. The mixture was stirred for 1 h and the water was evaporated under reduced pressure. The brown viscous liquid obtained was then dried under high vacuum. After drying, the product was cooled to room temperature at which point it crystallized. Suitable crystals for SCXRD were chosen from the product.

1-butyl-4-dimethylaminopyridinium chloride ([b4dmapy]Cl) was formed after reacting 50 g (0.41 mol) 4-(dimethylamino)pyridine with 43 mL (0.41 mol) 1-chlorobutane under reflux in ethyl acetate as described in the general procedure.

1-butyl-4-methylpyridinium bromide ([b4mpy]Br) was formed after reacting 227 mL (2.33 mol) 4-methylpyridine with 250 mL (3.08 mol) 1-bromobutane under reflux in ethyl acetate as described in the general procedure.

1-butyl-4-methylpyridinium hexafluorophosphate ([b4mpy][PF_6]) was formed after reacting 227 mL (2.33 mol) 4-picoline with 250 mL (3.08 mol) 1-bromobutane under reflux in ethyl acetate as described in the general procedure. Metathesis of the bromide salt to give the hexafluorophosphate salt was performed as described above.

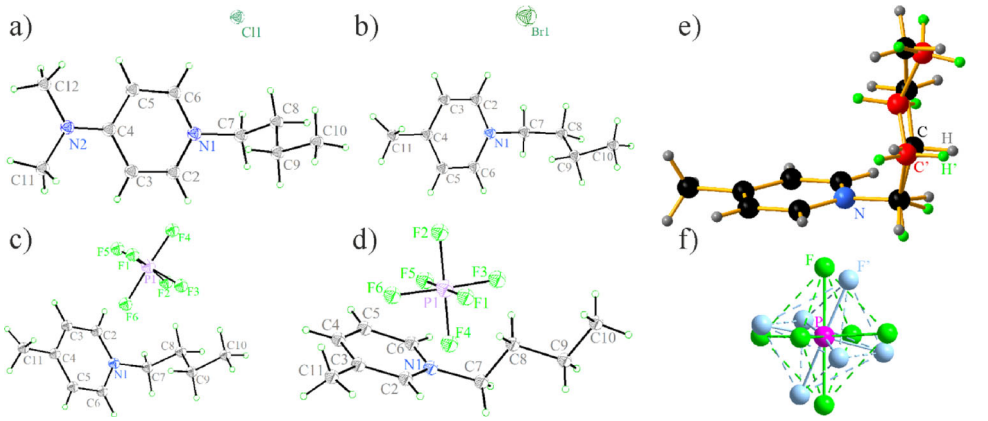

Figure 1. Formula units in the crystal structures of [b4dmapy]Cl (a), [b4mpy]Br (b, $Z'=2$), [b4mpy][PF_6] (c), and [b3mpy][PF_6] (d). Thermal ellipsoids are drawn at 50% probability for all atoms refined anisotropically. Disorder of the butyl chains in [b4mpy]Br (e) and [PF_6]$^-$ anions in [b4mpy][PF_6] (f).

1-butyl-3-methylpyridinium hexafluorophosphate ([b3mpy][PF_6]) was formed after reacting 250 mL (2.57 mol) 3-picoline with 269 mL (2.57 mol) 1-chlorobutane under reflux in ethyl acetate as described in the general procedure. Metathesis of the chloride salt to give the [PF_6]$^-$ salt was performed as described above.

Single-crystal X-ray diffraction. All of the compounds were structurally characterized. The X-ray data were collected on a Bruker SMART diffractometer equipped with a CCD area detector using graphite monochromated Mo-K_α ($\lambda = 0.71073$ Å) radiation. For each compound, a single crystal was mounted on a glass fiber and transferred to the goniometer for data collection. The crystals were cooled to $-100\,^{\circ}C$ under a cold nitrogen gas stream. The structures were solved using SHELX software [39, 40] and the absorption corrections were made with SADABS [41]. The structures were refined by full matrix least squares on F^2. All non-hydrogen atoms were readily located and their positions refined anisotropically. Hydrogen atom positions were added at idealized positions. Rotational disorder about the phosphorous was observed in the anions of both [b4mpy][PF_6] and [b3mpy][PF_6]. Disorder was also observed in the butyl tails of both molecules in the asymmetric units (A and B) of [b4mpy]Br. Both disorder components have been initially refined independently showing good correlation for the two symmetrically independent cations. Therefore, their occupations have been restricted to the same value upon final refinement.

3. Results and discussion

The formula units for the four single crystal structure determinations are presented in Figure 1. The butyl groups of both independent cations in the structure of [b4mpy]Br were found to be positionally disordered. The [PF_6]$^-$ anions in both [b4mpy][PF_6] and [b3mpy][PF_6] are rotationally disordered about the phosphorous. A comparison of the structurally related cations of the four crystal structures is provided in Table 1 (bond distances and angles), Figure 2 (cation tail conformations), and Table 2 (cation tail torsion angles).

Table 1. Selected bond angles (°) and distances (Å).

	[b4dmapy]Cl	[b4mpy]Br (A)[a]	[b4mpy]Br (B)[a]	[b4mpy][PF_6]	[b3mpy][PF_6]
Interior ring angle at heteroatom C2–N1–C6	119.3(1)	119.4(3)	120.1(3)	120.2(3)	121.9(5)
Interior ring angle at carbon C4–C5–C6	120.1(1)	120.8(4)	120.9(4)	120.6(4)	119.9(7)
Interior ring angle at substituent C3–C4–C5[b]	116.5(1)	116.8(3)	117.0(3)	117.5(3)	121.1(6)
Aromatic C–C Bond C5–C6	1.364(2)	1.361(6)	1.361(6)	1.370(5)	1.39(1)
Aromatic C–N Bond C2–N1	1.355(2)	1.354(5)	1.346(5)	1.344(4)	1.348(7)
Nonaromatic N–C Bond N1–C7	1.482(2)	1.479(5)	1.485(5)	1.485(5)	1.48(1)

[a]Values for the major conformation of the disorder are given first, followed by those for the minor conformation.

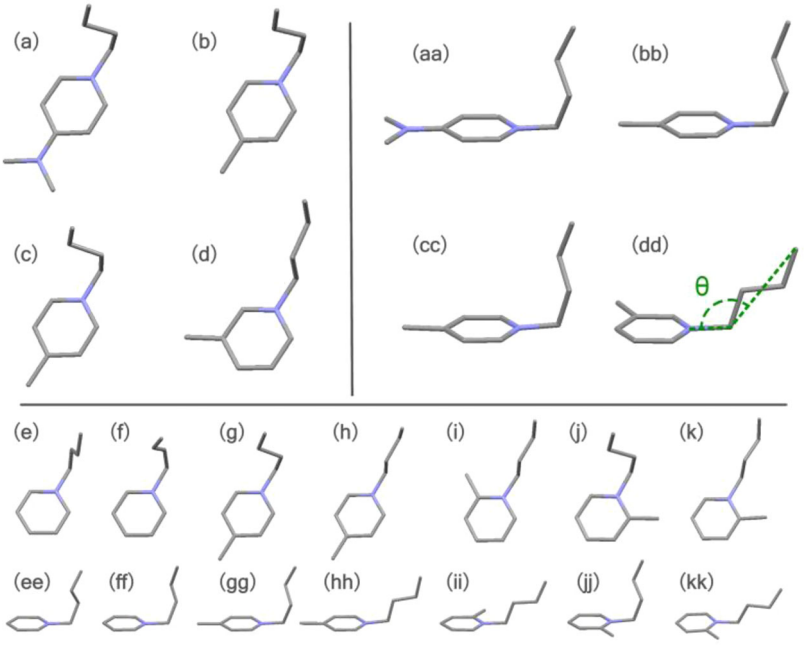

Figure 2. An overview of the butyl tail conformations of the cations of [b4dmapy]Cl, [b4mpy]Br, [b4mpy][PF_6], and [b3mpy][PF_6] viewed from above (a, b, c, and d, respectively) and from the side (aa, bb, cc, and dd, respectively). Below these are structures taken from the literature of the cations of 1-butylpyridinium chloride (e, ee) [29], 1-butylpyridinium bromide (f, ff) [32], *bis*(1-*n*-butyl-4-methylpyridinium) tetrachloropalladate(II) (g, gg, h, hh) [42], catena-(*bis*(*N*-n-butyl-2-methylpyridinium) hexakis(μ_2-iodo)-di-lead(II) dimethylformamide solvate monohydrate) (i, ii) [43], and catena-[*tris*(*N*-butyl-2-methylpyridinium) (μ_4-iodo)-tetrakis(μ_3-iodo)-tetrakis(μ_2-iodo)-hexa-silver(I)] (j, jj, k, kk) [44]. The torsion angles in the butyl tails, as well as, the N1–C7–C10 angle (θ) for (a) through (d) are given in Table 2.

3.1. Summary of the cation features

[b4dmapy]Cl. The angle (Table 1) made between the two methyl groups and the nitrogen of the para substituent is somewhat contracted at 119.3(1)°, indicating minor influence of the steric repulsion between the methyl groups and the nearest ring

Table 2. Descriptive angles of the butyl tail orientations (°).

Angle[a]	[b4dmapy]Cl	[b4mpy]Br (A)[b]	[b4mpy]Br (B)[b]	[b4mpy][PF_6]	[b3mpy][PF_6]
Torsion Angle N1–C7–C8–C9	60.2(2)	56(1), 41(3)	62(1), 38(1)	65.5(5)	171.3(5)
Torsion Angle C7–C8–C9–C10	173.9(2)	179(1), 175(2)	179(1), 178(1)	178.2(4)	179.2(6)
Tail Angle N1–C7–C10	101.9(1)	99.3(4), 104.7(4)	98.7(3), 105.6(4)	102.5(3)	131.9(4)

[a]Absolute values.
[b]Values for the major and minor conformation of the disorder, respectively.

atoms. The interior ring angle whose vertex is in the para position of the pyridine ring, C3–C4–C5, is also slightly compressed at 116.5(1)°. Two characteristic torsion angles (Table 2) of the butyl chains, N1–C7–C8–C9 and C7–C8–C9–C10, are 60.2(2) and 173.9(2)°, respectively. For [b4dmapy]$^+$, the first of these is gauche and the latter is anti (Figure 2). The N1–C7–C8–C9 torsion angle is responsible for rotating the tail back toward the cation, orienting it perpendicular to the plane of the pyridine ring and forcing the molecule to adopt an L shape. The N1–C7–C10 angle is a very steep 101.8(1)°. Despite having only one cation in the asymmetric unit, both + and – gauche tail conformations are observed.

[b4mpy]Br. Two conformations are possible by the gauche torsion angle about N1–C7–C8–C9. The angle is + gauche for the major disordered conformation of one cation of the asymmetric unit and -gauche for the major conformation of the other. However, the minor disordered conformation in each of them is oriented in the opposite direction. The second torsion angle (C7–C8–C9–C10) in the butyl tails approaches 180° for both unique cations in both conformations, leading to the same L shape observed in [b4dmapy]Cl. Some variety is seen in bond distances along the butyl tails, indicating the shortcomings of the simplistic disorder model employed to represent the large thermal motion present. The remainders of the cations, the rings, and substituents display a more consistent behavior. The interior bond angles of the pyridine rings are all roughly 120°, except the C3–C4–C5 bond angles, where the methyl groups are bonded. These angles are closer to 117°.

[b4mpy][PF_6]. The geometry of the pyridine ring is nearly ideal. All interior angles are roughly 120°, except where the methyl group attaches (117.5(6)°). The torsion angles along the butyl chain are again gauche and anti, respectively, leading to the usual L shape of the cation (∠N1–C7–C10 = 102.5(3)°).

[b3mpy][PF_6]. The geometry of the cation reveals insignificant distortion apparent in the bond angles of the pyridinium ring at the positions of the two substituents. The interior angle is larger at the heteroatom (122.3(7)°) but smaller at C3 (117.1(7)°), where the methyl group is attached, while the remaining interior ring angles are very near 120°. The C–C–C and N–C–C bond angles down the butyl chain are typical of alkyl chains and vary within 3σ around 111.0(7)°. The two torsion angles about the alkyl C–C bonds in the butyl chain are both anti. Consequently, the butyl tail bends away from the ring. The N1–C7–C10 angle between the chain and the plane of the pyridine ring is quite unusual – 132.0(5)°. The butyl tail of b3mpy$^+$ is very nearly in line with the C4–N1 axis, as well; it does not display the lateral kinking seen in the other three structures reported.

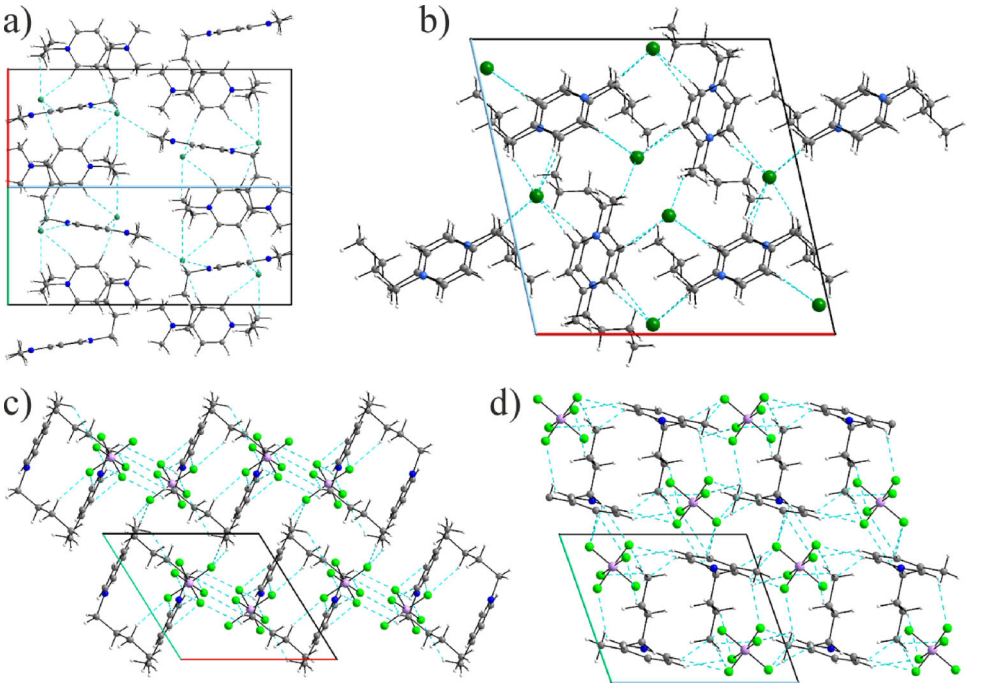

Figure 3. Crystal packing of [b4dmapy]Cl (a): [b4mpy]Br (b), [b4mpy][PF_6] (c), and [b3mpy][PF_6] (d). Only major disorder components have been presented for both the butyl chains and [PF_6]$^-$ anions for better clarity. Crystallographic axes are color-coded: *a* – red, *b* – green, *c* – blue. Hydrogen bonds are indicated with blue dashed lines.

3.2. Comparison of the cation features with the literature

One of the most common phenomena observed in these structures is the gauche orientation of the butyl tail within the cation with respect to the N1–C7 bond, leading to formation of the L shape of the cation. The gauche tail phenomenon was observed in the structure of 1-butylpyridinium chloride, which has no ring substitution on the cation other than the butyl tail [29], while in that of 1-butylpyridinium bromide the tail was found to have a nearly eclipsed N1–C7–C8–C9 torsion angle (8(4)°) [32]. A very similar picture has also been observed in the series of [PCl_6]$^-$ and [$NbCl_6$]$^-$ anions with different positions of the methyl group [36]. Interestingly all of the latter contain L-shaped cations, but each comes to this configuration through different means. The opposite case has been recently detected in the ortho-substituted 1-butyl-2-methylpyridinium bromide with the first torsion angle being anti and the second-gauche [37]. The latter case is strongly correlated with the efficient in plane packing including π–π pairs and van der Waals interactions between the ethyl groups of the butyl chains. Even more enlightening is the structure of bis(1-*n*-butyl-4-methylpyridinium) tetrachloropalladate(II) adopting simultaneously gauche and anti conformations of the butyl tail [42].

The *anti* torsion angles are unique for the [b3mpy]$^+$ cation. This conformation has been observed in the structure of catena-(*bis*(*N*-*n*-butyl-2-methylpyridinium) hexakis(μ_2-iodo)-di-lead(II) dimethylformamide solvate monohydrate [43]. However, the

Table 3. Selected anion–cation short contact distances (Å) and hydrogen bond angles (°).

[b4dmapy]Cl	Cl···H–C2	Cl···H–C3	Cl···H–C5	Cl···H–C6	Cl···H–C7	Cl···H–C7	Cl···H–C11
	2.69(1)	2.71(1)	2.69(1)	2.61(1)	2.83(1)	2.89(1)	2.66(1)
	159.9(1)	171.9(1)	157.8(1)	153.2(1)	151.0(1)	135.2(1)	172.9(1)
[b4mpy]Br (A)[a]	Br···H–C2	Br···H–C2	Br···H–C5	Br···H–C5	Br···H–C7	Br···H–C8	Br···H–C11
	2.707(1)	2.773(1)	2.771(1)	2.892(1)	3.058(1)	3.054(1)	2.971(1)
	162.2(2)	163.9(2)	167.7(2)	170.7(2)	122.3(2)	157.2(5)	152.2(2)
[b4mpy]Br (B)[a]	Br···H–C2	Br···H–C3	Br···H–C3	Br···H–C6	Br···H–C6		
	2.892(1)	2.752(1)	2.804(1)	2.713(1)	2.718(1)	2.871(1)	2.998(1)
	150.0(2)	168.2(2)	168.4(2)	164.8(2)	177.8(2)	148.6(2)	154.1(2)
[b4mpy][PF_6]	F1···H–C2	F6···H–C2	F5···H–C5	F6···H–C7	F6···H–C7	F4···H–C11	F1···H–C9
	2.66(1)	2.781(5)	2.843(5)	2.605(8)	2.467(5)	2.690(8)	2.539(4)
	173.9(3)	135.9(3)	115.5(2)	117.3(3)	156.7(3)	130.2(3)	129.6(3)
[b3mpy][PF_6]	F5···H–C6	F2···H–C7	F2···H–C6	F3···H–C5	F4···H–C2	F1···H–C7	F6···H–C11
	2.613(3)	2.516(5)	2.603(5)	2.536(6)	2.309(7)	2.556(3)	2.847(5)
	121.2(3)	153.8(4)	151.9(4)	135.2(4)	167.2(4)	150.3(3)	100.2(5)

[a]All close contacts occur to the atoms of the major conformations of disorder only.

structure of catena-[*tris*(*N*-butyl-2-methylpyridinium) (μ_4-iodo)-tetrakis(μ_3-iodo)-tetrakis(μ_2-iodo)-hexa-silver(I)] reported later [44] has three unique cations in the asymmetric unit, two of which display gauche conformation and one that displays the anti conformation. Examples of all three (gauche, anti, and eclipsed) conformations can be found in the CSD [45], yet there appears to be no straightforward dependency between substituent position and tail conformation showing a correlation at least to some degree on the anion and the position of the ring substituent. The gauche and eclipsed conformations give the cation an L-shape that can have significant effects on the packing preferences.

3.3. Summary of the supramolecular and packing features

The packing of **[b4dmapy]Cl** (Figure 3a) appears to be dominated by Coulombic attractions. However, the cations are arranged in a manner that suggests weak cation–cation interactions may have some influence on the structure. The cations stack parallel to the *ab* plane with their aromatic rings being practically orthogonal to each other and forming layers. The butyl and aminodimethyl tails stack pairwise parallel to each other and an identical pair from the neighboring layer being responsible for formation of the hydrophobic areas in the interlayer space. The closest distances between these tails significantly exceeds the sum of the van der Waals radii pointing to very weak interactions. In addition, the butyl tails point toward the point of substitution (C4) of another cation suggesting similar nonbonding C–H···C π interactions. Each cation has seven short contacts made to five chloride anions with the directional nature suggesting that mostly classical hydrogen bonds are occurring (Table 3). Four of these occur between the hydrogen atoms of aromatic carbons within the ring. The anions interact with seven hydrogen atoms of five cations showing strong preference for the aromatic or methyl/α-methylene H positions.

The packing of **[b4mpy]Br** is also salt-like in nature and contains certain similar features with [b4dmapy]Cl, including pseudo-layered motifs. The position of the methyl and butyl tails alternate along the *b* direction in a zigzag manner, while the mutual orientation of the cations alternates at 90° along the *a* and the *c* axes. Due to such orientation, there are no apparent hydrophobic areas as all carbon tails from both

layers share the interlayer space with the anions. Both cations make close contacts to six anions. Again, most of these interactions are directional in nature and include all hydrogen atoms of the aromatic carbons, and methyl/α-methylene groups (Table 3). The anions also interact with six different cations allowing for multiple bonds to the same cation. There is no anion-ring centroid interaction observed in the structure as well as no apparent π–π interactions between the cations. Only weak nonbonding C–H···π contacts could be observed involving longer carbon tails similarly to [b4dmapy]Cl playing negligible role in the total bonding picture.

The molecular packing in **[b4mpy][PF_6]** reveals increased influence of hydrogen bonding interactions, while isolated hydrophobic areas could still be observed (Figure 2c). Cation–cation interactions are limited to head-to-tail and tail-to-tail interactions, and no π–π stacking or edge-to-face interactions have been observed. The head-to-tail interactions help to align the L-shaped cations in single-file rows, with anions occupying the rectangular wells formed in this arrangement. The tail-to-tail interactions occur between butyl tails of the cations from the neighboring rectangles. Seven out of twelve C–H···F interactions occur to carbon atoms adjacent to the nitrogen and the same amount to the nonaromatic carbons in big contrast to the former structures. The angles of these bonds are widely distributed between 115 and 174° showing less directional character. There are a few lp···π contacts between the fluorine atoms and the ring carbons, but the relatively large distances indicate that these are not an anion-ring centroid interaction. Having identical number of short F···H contacts (12) anions are surrounded by six cations, while cations – by seven anions.

The packing of **[b3mpy][PF_6]** is also of a typical salt fashion (Figure 3d). There do not appear to be any substantial channels through or pockets within the lattice. Tail-to-tail interactions are responsible for the relatively isolated cationic pairs stacking along the *a* axis. There exists no obvious π–π stacking or edge-to-face cation-cation interactions, as well as no anion–π interactions. However, the methyl substituent of the cation resides directly over the centroid of the ring of an adjacent cation, at a distance of 3.663 Å. Necessarily, the methyl group of the adjacent cation lies directly under the centroid of the ring of the first cation. If this arrangement is to be considered a real interaction, which is questionable given the distance, each set of two cations may be thought of as a dimer, held together by these carbon-ring interactions. All other obvious close contacts exist between the cation and the anion. There exist 16 C–H···F interactions between the cation and the surrounding anions covering practically all H positions with slight preference for the aromatic carbon positions and those directly bonded to the nitrogen. Each cation is surrounded by seven anions and *vice versa*. All these interactions occur at a relatively large angle distribution, similar to that observed in [b4mpy][PF_6] (100.2(5)–167.2(4)°).

3.4. Consideration of the role in solvation and crystallization

For the halide salts, **[b4dmapy]Cl** and **[b4mpy]Br**, there is a moderate amount of strongly directional cation–anion hydrogen bonds and an enhanced amount of cation–cation interactions (C-H···C π and van der Waals) which lead to the network formation with rotational checkered motifs. These contacts show strong preference to

the more acidic hydrogen positions of the aromatic ring and those directly adjacent to the N atoms [46]. The $[PF_6]^-$ salts show instead a higher density of longer and less directional hydrogen bonds with no H-position preference. The hydrogen bond frustration observed in the latter compounds correlates well with the considerably lower melting temperatures of the $[PF_6]^-$ compared to the halide salts [47]. In addition, the nature of the cation–cation contacts also has to be taken into consideration. Inter-cationic contacts are less visible, represented by weaker van der Waals interactions and show lower dimensional (1D) arrangements compared to the stronger C–H···C π interactions in the halide salts.

When considering how these compounds may behave as crystallization solvents, the crystal structures illustrate an overall lack of strong, highly conserved interactions. As solvents, the anions of these ILs can be expected to dominate interactions with solutes, an effect which has been reported in investigations on the interactions of pyridinium ILs with both small molecule [48] and polymeric solutes [49]. As for the crystallization process itself, the pyridinium cations display great plasticity, being able to support lattices with much smaller counterions, such as Cl^-, or much larger ones as observed in their salts with lanthanide saccharinate complex anions [26]. A distinctly nonsymmetrical L-shape is highly conserved among butylpyridinium salts and has an apparently uniformly weakly acidic surface. This contrasts with other more commonly used IL counterions such as tetraalkylammonium, which tends to be more symmetrical, or dialkylimidazolium, where the strongest interactions are associated with the planar core. We anticipate these features would be useful in the crystallization of ionic coordination polymers, where the weakly solvated anions initially interact with metal ions to form small, mobile species that are able to assemble in solution with the pyridinium ions acting as supramolecular templates. The shape and behavior of the cation may also make it particularly effective in stabilizing discrete metal complexes with large anionic ligands, where the cation can use its shape to wrap around the ligands and buffer the anion–anion repulsion.

4. Conclusions

The crystal structures of two ionic liquid precursors based on hard halogen anions, [b4dmapy]Cl and [b4mpy]Br, and those of two ionic liquids based on the soft $[PF_6]^-$ anion, [b4mpy][PF_6] and [b3mpy][PF_6], have been closely examined. The cations of the halide salts form strong interactions with one another and assemble in extended networked chains. Lower dimensional cation assemblies were also observed in the case of the $[PF_6]^-$ salts, but the interactions linking the cations are of the weaker van der Waals variety. The cation–anion interactions within the structures of the halide salts are highly directional and represent classical hydrogen bonds. These contacts show strong preference for the position of interaction in the pyridine ring of the cation. Conversely, the cation–anion contacts in the structures of the $[PF_6]^-$ salts show no position preference and occur to practically all positions even of the butyl chain. The angles of these contacts are smaller, pointing to weaker and less directional interactions. The decreased symmetry of $[b3mpy]^+$ has substantial influence on the cation–-cation linking but does not overcome the influence of the much stronger

cation–anion interactions. The role of the cation in crystallizations can be traced to its shape and weakly acidic character, which gives it structure-ordering rigidity but allows it to accommodate anions of wide-ranging sizes.

Acknowledgements

The authors would like to thank the many students of The University of Alabama's CH605, Introduction to X-ray Crystallography, who discussed and described these data over many classes, including L. Block, E. C. Ellingsworth, A. L. Glover, C. S. Griggs, T. C. Mikulas, C. J. Saint-Louis, and Z. Shan.

Disclosure statement

No potential conflict of interest was reported by the authors.

Funding

This research was supported, in part, by the Royal Swedish Academy of Science through the Göran Gustafsson prize to A.-V.M., SSF, the Swedish Foundation for Strategic Research through the REFIT project (A.-V.M.) and by a Tage Erlander Guest Professorship to R.D.R. (VR Grant 2018-00233).

ORCID

Steven P. Kelley http://orcid.org/0000-0001-6755-4495
Volodymyr Smetana http://orcid.org/0000-0003-0763-1457
Anja-Verena Mudring http://orcid.org/0000-0002-2800-1684
Robin D. Rogers http://orcid.org/0000-0001-9843-7494

References

[1] T. Welton. *Biophys. Rev.*, **10**, 691 (2018).
[2] J.P. Hallett, T. Welton. *Chem. Rev.*, **111**, 3508 (2011).
[3] R. Kore, P. Berton, S.P. Kelley, P. Aduri, S.S. Katti, R.D. Rogers. *ACS Catal.*, **7**, 7014 (2017).
[4] I. Billard, A. Ouadi, C. Gaillard. *Anal. Bioanal. Chem.*, **400**, 1555 (2011).
[5] X. Sun, H. Luo, S. Dai. *Chem. Rev.*, **112**, 2100 (2012).
[6] D. Prodius, M. Klocke, V. Smetana, T. Alammar, M. Perez Garcia, T.L. Windus, I.C. Nlebedim, A.-V. Mudring. *Chem. Commun.*, **56**, 11386 (2020).
[7] E.R. Parnham, R.E. Morris. *Acc. Chem. Res.*, **40**, 1005 (2007).
[8] T.P. Vaid, S.P. Kelley, R.D. Rogers. *IUCrJ*, **4**, 380 (2017).
[9] Y. Yoshida, G. Saito. *Phys. Chem. Chem. Phys.*, **12**, 1675 (2010).
[10] D. Prodius, A.-V. Mudring. *Coord. Chem. Rev.*, **363**, 1 (2018).
[11] A.V. Mudring, A. Babai, S. Arenz, R. Giernoth. *Angew. Chem. Int. Ed. Engl.*, **44**, 5485 (2005).
[12] S.P. Kelley, V. Smetana, S.D. Emerson, A.-V. Mudring, R.D. Rogers. *Chem. Commun. (Camb.))*, **56**, 4232 (2020).
[13] A.E. Visser, R.P. Swatloski, W.M. Reichert, S.T. Griffin, R.D. Rogers. *Indus. Eng. Chem. Res.*, **39**, 3596 (2000).
[14] M.P. Jensen, J.A. Dzielawa, P. Rickert, M.L. Dietz. *J. Am. Chem. Soc.*, **124**, 10664 (2002).

[15] I. Billard, A. Ouadi, E. Jobin, J. Champion, C. Gaillard, S. Georg. *Solvent Extr. Ion Exch.*, **29**, 577 (2011).
[16] T. Vander Hoogerstraete, K. Binnemans. *Green Chem.*, **16**, 1594 (2014).
[17] S.I. Nikitenko, C. Cannes, C.L. Naour, P. Moisy, D. Trubert. *Inorg. Chem.*, **44**, 9497 (2005).
[18] C. Gaillard, O. Klimchuk, A. Ouadi, I. Billard, C. Hennig. *Dalton Trans.*, **41**, 5476 (2012).
[19] Y. Umebayashi, T. Mitsugi, S. Fukuda, T. Fujimori, K. Fujii, R. Kanzaki, M. Takeuchi, S.-I. Ishiguro. *J. Phys. Chem. B.*, **111**, 13028 (2007).
[20] B. Mallick, H. Kierspel, A.-V. Mudring. *J. Am. Chem. Soc.*, **130**, 10068 (2008).
[21] C.C. Hines, D.B. Cordes, S.T. Griffin, S.I. Watts, V.A. Cocalia, R.D. Rogers. *New J. Chem.*, **32**, 872 (2008).
[22] V. Smetana, S.P. Kelley, H.M. Titi, X. Hou, S.-F. Tang, A.-V. Mudring, R.D. Rogers. *Inorg. Chem.*, **59**, 818 (2020).
[23] F.S. Oliveira, E.J. Cabrita, S. Todorovic, C.E.S. Bernardes, J.N. Canongia Lopes, J.L. Hodgson, D.R. MacFarlane, L.P.N. Rebelo, I.M. Marrucho. *Phys. Chem. Chem. Phys.*, **18**, 2756 (2016).
[24] R.A. Carpio, L.A. King, R.E. Lindstrom, J.C. Nardi, C.L. Hussey. *J. Electrochem. Soc.*, **126**, 1644 (1979).
[25] S. Sowmiah, J.M.S.S. Esperança, L.P.N. Rebelo, C.A.M. Afonso. *Org. Chem. Front.*, **5**, 453 (2018).
[26] S.-F. Tang, A.-V. Mudring. *Inorg. Chem.*, **58**, 11569 (2019).
[27] T.S. Eike, E. Edengeiser, B. Mallick, M. Havenith, A.-V. Mudring. *Chem. Eur. J.*, **20**, 5338 (2014).
[28] C.R. Groom, I.J. Bruno, M.P. Lightfoot, S.C. Ward. *Acta Crystallogr. B Struct. Sci. Cryst. Eng. Mater.*, **72**, 171 (2016).
[29] D.L. Ward, R.R. Rhinebarger, A.I. Popov. *Acta Crystallogr. C Crystallogr. Struct. Commun.*, **42**, 1771 (1986).
[30] B.P. Regmi, F.R. Fronczek, I.M. Warner. *CSD Commun.*, 1937660 (2019).
[31] M. Konno, Y. Saito. *Acta Crystallogr. B Struct. Crystallogr. Cryst. Chem.*, **37**, 2034 (1981).
[32] J.-X. Ji, B. Xu, S. Liu, J.-T. Wang. *Acta Crystallogr. E Struct. Rep. Online*, **62**, o516 (2006).
[33] C.-Y. Pan, L.-J. Zhong, J. Lu, D.-G. Li, F.-H. Zhao, H.-M. Yang. *Z Anorg. Allg. Chem.* , **640**, 352 (2014).
[34] S.A. Suarez, A. Foi, S. Eady, A. Larsen, F. Doctorovich. *Acta Crystallogr. C*, **67**, o417 (2011).
[35] J. Dymon, R. Wibby, J. Kleingardner, J.M. Tanski, I.A. Guzei, J.D. Holbrey, A.S. Larsen. *Dalton Trans.*, 2999 (2008).
[36] M. Gjikaj, J.-C. Leye, T. Xie, W. Brockner. *CrystEngComm.*, **12**, 1474 (2010).
[37] M. Hog, M. Schneider, I. Krossing. *Chemistry*, **23**, 9821 (2017).
[38] S. Weber, J. Brünig, V. Zeindlhofer, C. Schröder, B. Stöger, A. Limbeck, K. Kirchner, K. Bica. *ChemCatChem*, **10**, 4386 (2018).
[39] G. Sheldrick. *Acta Crystallogr. C Struct. Chem.*, **71**, 3 (2015).
[40] G. Sheldrick. *Acta Crystallogr. A Found Adv.*, **71**, 3 (2015).
[41] L. Krause, R. Herbst-Irmer, D. Stalke. *J. Appl. Crystallogr.*, **48**, 1907 (2015).
[42] W. Zawartka, A. Gniewek, A.M. Trzeciak, Ł. Drzewiński, T. Lis. *Acta Crystallogr. E Struct. Rep. Online*, **62**, m1100 (2006).
[43] H. Li, Z. Chen, C. Huang, Z. Lian, J. Chen. *Chin. J. Inorg. Chem.*, **20**, 703 (2004).
[44] H.-H. Li, Z.-R. Chen, J.-Q. Li, C.-C. Huang, X.-L. Hu, B. Zhao, Z.-X. Ni. *J. Clust. Sci.*, **16**, 537 (2005).
[45] F. Allen. *Acta Crystallogr. B*, **58**, 380 (2002).
[46] R. Ahuja, A.G. Samuelson. *Crystallogr. Eng. Commun.*, **5**, 395 (2003).
[47] W. Haynes. *CRC Handbook of Chemistry and Physics*, Taylor and Francis Group LLC, London (2015).
[48] I.C.M. Vaz, M. Bastos, C.E.S. Bernardes, J.N. Canongia Lopes, L.M.N.B.F. Santos. *Phys. Chem. Chem. Phys.*, **20**, 2536 (2018).
[49] E.S. Sashina, D.A. Kashirskii, E.V. Martynova. *Russ. J. Gen. Chem.*, **82**, 729 (2012).